The time-of-flight estimation accuracy versus digitization parameters

L.Svilainis, V. Dumbrava

Signal processing department, Kaunas University o f Technology,

Studentu str. 50, LT-51368 Kaunas, Lithuania, tel. +370 37 300532, E-mail.:svilnis@ktu.lt

Abstract

   The accuracy of the time delay estimation using the direct correlation technique has been theoretically calculated.
   The random errors of the time delay estimation in digital ultrasonic measurement systems have been studied. The techniques for the time-of-flight (ToF) estimation have been discussed. The theoretical equations for analog and discrete case are presented. Numerical simulation has been carried out. The ToF estimation was performed using the direct correlation technique. Numerical simulation analyzed the influence of additive white Gaussian noise power spectral density, ultrasonic signal bandwidth, carrier frequency, analog-to-digital converter sampling frequency and resolution.
Keywords: Ultrasonic measurements, time-of-flight estimation, data acquisition, acoustic signal processing.

Introduction

   The time-of-flight (ToF) estimation is quite recent task in ultrasonic measurements. The ToF is the time needed for an ultrasonic wave to travel a certain distance. For instance from a transmitter to a target and then, after reflection, back to the receiver located near the transmitter [1, 2]. Usually ratio frequency (RF) pulse is used for that purpose.

   In simple applications, where accuracy is not an issue the ToF is computed using the threshold method: the echo signal arrival time is assigned at certain amplitude level crossing. This technique is so simple that only analog comparator and counter are sufficient to get reasonable results. There is a variety of specialized sensors for time interval to code conversion. For instance, TDC-GP1 offers 2 measuring channels with 250 ps resolution each and a basic measurement range of 15 bit [3]. The threshold technique offers a low cost and simple solution, but suffers from poor accuracy: the measured time delay depends on the intensity of the echoes, or rather, on the object's nature, size, and distance from the transducer [1, 4, 5].

   The more complex signal processing techniques can be applied in order to get much higher accuracy [6-8]. Signal has to be converted to a digital form in order to apply the digital signal processing.

   The digitization of the ultrasonic signals is offering a flexible signal processing. A big variety of processing techniques can be applied. The digitization parameters are important during such systems design [9]. The designers usually do not address this problem properly. Typically sampling frequency and resolution are chosen "as high as possible", but such approach will raise the system costs. So, it is preferred to have a lower sampling frequency, window size and resolution of analog-to-digit converter (ADC). Some publications analyze the choice of sampling parameters [10, 11]. However, in many publications the signal often is treated as a continuous wave (CW). The ultrasonic ToF estimation frequently uses a pulse signal. The task of this article is to determine the theoretical ToF estimation accuracy for digital ultrasonic systems using pulse signals. This paper is presenting the results of carried out investigation.

The ToF measurement methods

   The ultrasonic system is using the ToF for a distance estimation. The distance can be estimated as:

$$l = \frac{v(ToF)}{2},\qquad(1)$$

where v represents the sound propagation velocity, ToF is the delay time. It can be seen that the range of the measurement accuracy depends on the ToF and the sound velocity v accuracy. We shall concentrate on the ToF estimation accuracy. The complex digital signal processing is assumed to be used for the ToF estimation.

   The echo received signal $s_R(t)$ can be treated as a delayed and attenuated version of the transmitted signal $s_T(t)$ with an additive white noise added:

$$s_R(t) = A(t) \cdot s_T(t - \text{ToF}) + n(t),\qquad(2)$$

where $A(t)$ is the attenuation function and $n(t)$ is an additive white Gaussian noise (AWGN) with the power spectral density N_0. Additionally it is assumed that the noise signal is not correlated with the signal. The AWGN power spectral density N_o can be obtained from the noise waveform standard deviation in the time domain and the bandwidth B ratio:

$$N_0 = \frac{\sigma[n(t)]^2}{B}.\qquad(3)$$

   The problem of the ToF estimation is to find an estimate of the true position of the signal arrival using the noisy received signal. Three ToF estimation techniques have been indicated in [1, 5, 12]: the direct correlation maximization, the L2 norm minimization and the L1 norm minimization.

   The direct correlation technique is using position of the peak of the cross-correlation function R_{DC} as the signal arrival position (so the ToF) estimate:

$$ToF_{DC} = \arg[\max R_{DC}(\tau)],\qquad(4)$$

where R_{DC} is:

$$R_{DC}(\tau) = \int_{-\infty}^{\infty} s_T(t) \cdot s_R(t - \tau)dt.\qquad(5)$$

   The L2-norm minimization technique or average square difference function estimator is using the position

where L2-norm of the received signal and the reference signal is minimal:

$$ToF_{L2} = \arg\{\min[L2(\tau)]\},\qquad(6)$$

where L2 is:

$$L2(\tau) = \int_{-\infty}^{\infty}[s_R(t) - s_T(t-\tau)]^2\,dt\,.\qquad(7)$$

The L1-norm or average magnitude difference function is using the position where the L1-norm of received signal and the reference signal is minimal:

$$ToF_{L1} = \arg\{\min[L1(\tau)]\},\qquad(8)$$

where L1 is:

$$L1(\tau) = \int_{-\infty}^{\infty}|s_R(t) - s_T(t-\tau)|\,dt\,.\qquad(9)$$

The direct correlation technique possesses the optimal filter properties and broad theoretical analysis is done on the ToF estimation variance [1, 5, 13-15]. Therefore, it has been chosen for this analysis. The variance of the ToF standard deviation is given by [14]:

$$\sigma(TOF) \geq \frac{1}{F_e\sqrt{\dfrac{2E}{N_0}}}\,.\qquad(10)$$

where E is the signal $s_T(t)$ energy, F_e is the effective bandwidth of the signal. The signal energy can be calculated either using signal temporal presentation or the signal spectral density (SSD) $S(f)$:

$$2E = \int_{-\infty}^{\infty}|s_T(t)|^2\,dt = 2\int_0^{\infty} S(f)\cdot S^*(f)\,df\,.\qquad(11)$$

The effective bandwidth of the ultrasonic RF signal can be calculated as [14]:

$$F_e{}^2 = \frac{\displaystyle\int_{-\infty}^{\infty}(2\pi f)^2|S(f)|^2\,df}{2E} + \frac{\left[2\pi\displaystyle\int_{-\infty}^{\infty}f|S(f)|^2\,df\right]^2}{E^2}\,.\qquad(12)$$

The equations presented above are dealing with analog signals. The conversion of these equations into a discrete form is needed. The transformations of the analog signal occurring due to sampling effect are discussed in the next chapter.

The digitization process

The analog signal $s(t)$ sampling with the period T_s can be presented as multiplication of an analog signal $s(t)$ with a delta impulse train [16] termed as a *shah* function III or *Dirac comb*:

$$x(nT_s) = s(t)\cdot III(t, T_s)\,.\qquad(13)$$

The *shah* function is a periodic Schwartz distribution constructed from the Dirac delta functions $\delta(t)$:

$$III(t, T_s) = \sum_{k=-\infty}^{\infty}\delta(t - kT_s)\,.\qquad(14)$$

The Fourier transform of this function is also *shah* function. If multiplication in the time domain corresponds to convolution in the frequency domain, then the sampled signal spectrum will be periodical with a period of the sampling frequency f_s. The aliasing will occur for any frequency component (both signal and noise) falling outside the $f_s/2$. For baseband signals the region between zero and the $f_s/2$ is addressed as the Nyquist zone. For this reason the antialiasing filter is used in almost all ADC applications [9]. The filter passband with the maximum cut-off frequency f_a should not corrupt the signal being recorded. The stopband attenuation at frequencies $f_s - f_a$ has to be equal to the dynamic range (DR) of the signal (refer to Fig.1).
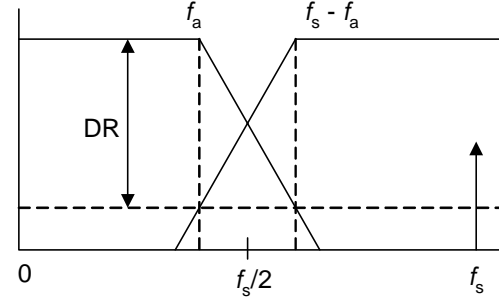

Fig 1. **Anti-aliasing filter requirements**

The DR usually is defined as CW signal RMS level E_{RX} and the total noise RMS level's E_{ntot} ratio at the input ADC:

$$DR = 20\lg\left(\frac{E_{RX}}{E_{ntot}}\right).\qquad(15)$$

The E_{RX} is calculated using the ADC analog signal input swing $V_{ADCp\text{-}p}$:

$$E_{RX} = \frac{V_{ADCp-p}}{2\sqrt{2}}\,.\qquad(16)$$

The ADC quantization noise is calculated by using the quantization step q which in turn is obtained from the ADC resolution b in bits and the analog signal input swing $V_{ADCp\text{-}p}$:

$$E_{nADC} = \frac{q}{\sqrt{12}} = \frac{V_{ADCp-p}}{2^N\sqrt{12}}\,.\qquad(17)$$

The total noise level is taking into account both the ADC quantization noise E_{nADC} and the amplifier intrinsic noise E_{nAMP}:

$$E_{n\,tot} = \sqrt{E_{nADC}^2 + E_{nAMP}^2}\,.\qquad(18)$$

Amplifier intrinsic noise is calculated by integrating the noise density e_n over the passband frequency range:

$$E_{nAMP} = \sqrt{\int_0^{f_a} e_n^2\,df}\,.\qquad(19)$$

The analysis of the ultrasonic preamplifier noise model and the total noise calculations can be found in [17].

The ToF accuracy estimation for digital signal

Variety of publications use the numerical simulation to verify the improved ToF estimation techniques [1, 5-7]. Signal is sampled as given by Eq. 13 and the discrete cross-correlation is calculated:

$$M = \arg\{\max[DC_k]\},\qquad(20)$$

where

$$DC_k = \frac{1}{N} \sum_{n=1}^{N} rx_n \cdot tx_{n-k}, \qquad (21)$$

where rx_n and tx_n are the discrete arrays obtained after signal sampling for received and transmitted (reference) signals respectively. The ToF estimator then will have some granularity defined by the sampling frequency f_s. The ToF precision will be significantly influenced by choice of the sampling frequency. Increase of the sampling frequency will increase the system cost and the processing time. For significant SNR the accuracy can be increased by a parabolic interpolation technique [18] or combination of the Hilbert transform and the linear interpolation [19]. More advanced interpolation techniques can be found in [6]. The parabolic approximation:

$$R_{DC}^{\#}(\tau) = a_0 + a_1\tau + a_2(\tau)^2, \qquad (22)$$

is using the sample of a maximum amplitude and the two samples surrounding it (Fig.2).
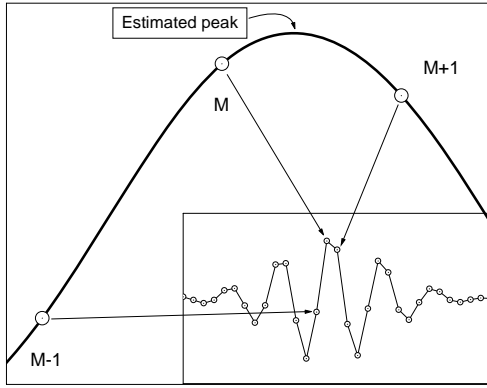

Fig. 2. **The parabolic interpolation for TOF estimation**

The positions M-1, M and M+1 that are used can be solved to find the parabolic equation for apex:

$$ToF_{DC}^{\#} = -\frac{a_1}{2a_2} = \frac{DC_{M-1} - DC_{M+1}}{2(DC_{M-1} - DC_M + DC_{M+1})}. \qquad (23)$$

The parabolic interpolation has been chosen for further investigation thanks to simplicity of this technique.

We suggest using the digital signal record to estimate the ToF variance. For such purpose analytical Eq. 3, 10, 11 and 12 have to be adopted for a discrete signal nature. The $N_0^{\#}$ is calculated using the Nyquist frequency and the noise standard deviation $\sigma^{\#}$:

$$N_0^{\#} = \frac{(\sigma^{\#})^2}{f_s / 2}. \qquad (24)$$

The approximate estimation of SSD can be calculated using the discrete Fourier transform (DFT):

$$X_k = F\{x[k]\} = T_s \sum_{n=1}^{N-1} x_n \cdot e^{-j2\pi kn/N}. \qquad (25)$$

Then the energy of the signal can be obtained:

$$E^{\#} = \frac{f_s}{N} \sum_{k=0}^{N} X_k \cdot X_k^*. \qquad (26)$$

Using X_k the centroid of SSD can be calculated:

$$f_0 = \frac{2f_s}{E'N} \sum_{k=1}^{N/2} F_k X_k \cdot X_k^*, \qquad (27)$$

where

$$F_k = \frac{(k-1)\cdot f_s}{N}. \qquad (28)$$

The quantity β is:

$$\beta = 2\pi \sqrt{\frac{f_s}{E^{\#}N} \sum_{k=1}^{N/2} (F_k - f_0)^2 \cdot X_k \cdot X_k^*}. \qquad (29)$$

Then the effective bandwidth of the ultrasonic RF signal is:

$$F_e^2 = \beta^2 + (2\pi f_0)^2. \qquad (30)$$

The ToF estimation is obtained using Eq.10.

The numerical simulation

The numerical simulation has been carried out in order to evaluate the influence of the sampling parameters on a ToF estimation performance. The signal has been simulated as CW with the Gaussian envelope and amplitude of unity:

$$s_T(t) = e^{-\alpha t^2} \cos(2\pi f_C t), \qquad (31)$$

where α, is related to the transducer bandwidth and f_C is the transducer center frequency.

The goal of the numerical simulation was to reveal the influence of SNR, sampling frequency and ADC resolution on random errors of the ToF estimation. The simulation has been carried out using MATLAB. Random errors of the ToF have been obtained by taking a large number of runs (more than 1000) and obtaining the standard deviation of the ToF value estimated. The noise has been simulated using *randn* function. The sampled and noisy version of the received signal can be written as:

$$s_R(nT_s) = e^{-\alpha(nT_s - ToF)^2} \cos[2\pi f_C(nT_s - ToF)] + \sigma^{\#} \cdot randn. \qquad (32)$$

The SNR has been varied by changing the multiplier $\sigma^{\#}$ of *randn* function. The signal power spectral density obtained from a single measurement and after one million runs RMS averaging are presented in Fig.3.
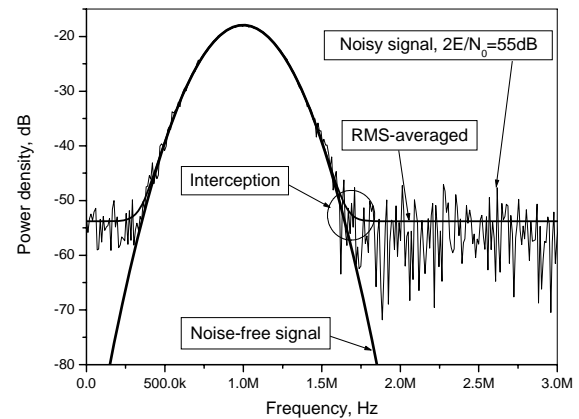

Fig. 3. **The power spectral density of the simulated signal**

The results have been obtained using the 1 MHz center frequency and the 0.5 MHz bandwidth (-3 dB) transducer model. In order to investigate the sampling frequency

influence on the ToF estimation the sampling frequency has been varied from 1 MHz to 100 MHz. The lowest sampling frequency was deliberately chosen to be twice the bandwidth. In the case of proper undersampling this frequency will hold as a Nyquist higher order zone [9]. The aim was to evaluate the sampling frequency and the aliasing influence on the variance of TOF. Three types of experiments have been carried out:

    a) no antialiasing filter,
    b) antialiasing filter,
    c) only antialiasing filter.

    The results obtained are presented in Fig.4.
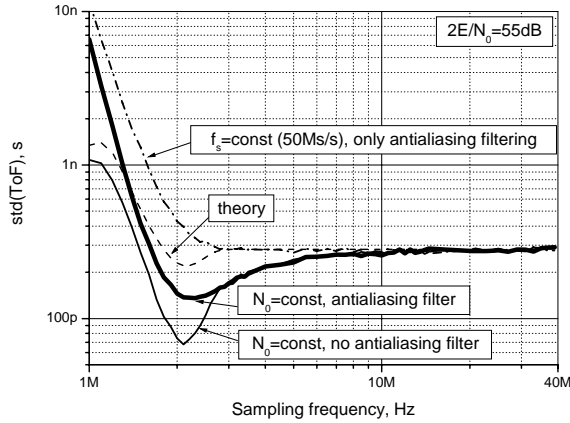
Fig. 4. **The power spectral density of the simulated signal**

For case a) (no antialiasing filter) the signal sampling was simulated using Eq. 32. The noise power spectral density N_o after sampling was maintained at the same level. This has been done by regulating the multiplier $\sigma^{\#}$ of the *randn* function:

$$\sigma_{norm}^{\#} = \sigma^{\#}\sqrt{\frac{f_s}{f_{snorm}}}, \qquad (33)$$

where f_{snorm} is the 100 MHz sampling frequency. Theoretical calculation of ToF variance for case a) using Eq. 10, 22-30 has been done for every sampling rate f_s.

For case b) (antialiasing filter) the signal has been sampled at a sufficiently high frequency f_{snorm} and then resampled using MATLAB function *resample* to get the signal at lower rate f_s. This command applies an antialiasing (lowpass) FIR filter to the input signal during the resampling process, and compensates for the filter's delay.

For case c) the signal was sampled at a sufficiently high frequency f_{snorm} and only the antialiasing filter applied.

In all cases measures were taken to maintain the constant level of the noise power spectral density N_o. At high sampling frequencies the ToF variance behaved as expected: a, b c and theory curves match. But for sampling rates approaching the noise and signal power density interception point indicated in Fig.3 there is a reduction of the ToF random errors. This reduction can be noted on experiments where aliasing can occur: cases a and b. There is no reduction for case c), where only the filter is applied. One can assume that the normality of the errors distribution is distorted. In order to check the normality of the ToF errors distribution lag plots for various f_s

frequencies have been analyzed. No indication of deviation from normality was noted. Refer to Fig. 5 for the ToF lag plot at the sampling rate of 2.1 MHz.
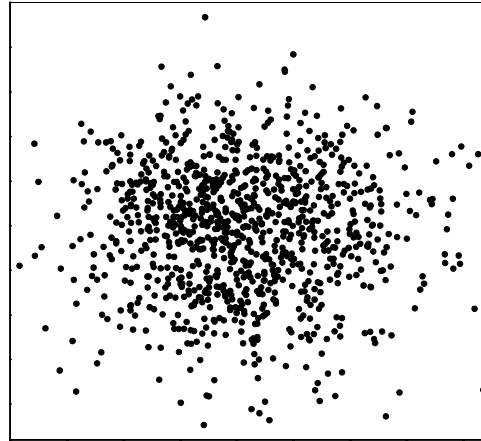

Fig. 5. **Lag-plot of the ToF values for f_s =2.1 MHz case a).**

The carrier frequency has a significant influence on the effective bandwidth. This can be seen when analyzing Eq.30: for narrowband signals the f_0 (centroid of the SSD) should prevail. The f_0 actually is the carrier frequency f_c. The influence of the carrier frequency on the ToF estimation performance has been investigated.

The carrier frequency has been varied from 0.3 to 3 MHz. For the 5 MHz sampling frequency the upper value is close to undersampling, but the higher order Nyquist zone is still applicable since the bandwidth 0.5 MHz was maintained. The results in Fig.6 are in a good agreement with Eq. 10 and 30: the increase of the carrier frequency is causing reduction of random errors.
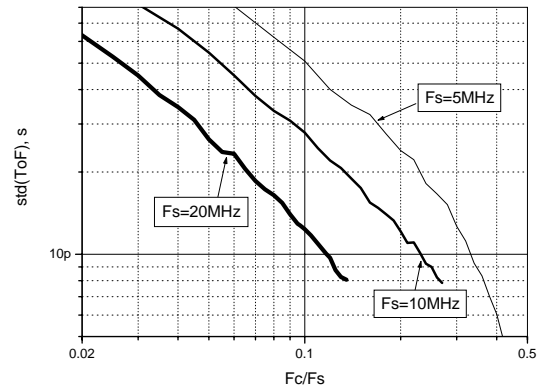

Fig. 6. **Influence of carrier frequency on the ToF random errors case a.**

The simulation has been carried out to investigate the influence of bandwidth on sampling parameters.

The pulse duration has been varied in order to get the 0.1MHz, 0.2MHz, 0.5MHz, 1MHz and 2MHz bandwidth signals. The results of the ToF standard deviation versus the ADC sampling rate are presented in Fig.7 (case a) and Fig.8 (case b).

The results in Fig.7 are significantly different from ones presented in Fig.8 for wide bandwidth simulations. This can be explained by antialiasing effect of the filter present in the case b. Therefore, there is no ringing of the

curve obtained at a wide bandwidth in Fig.8, but the ringing is present in Fig.7.
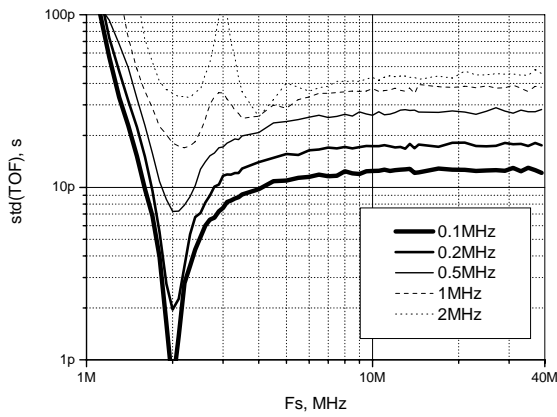

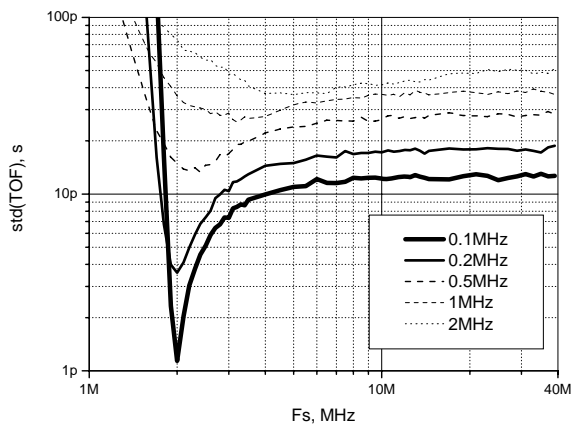Fig. 7. **Bandwidth influence on the ToF random errors, case a.**

Fig. 8. **Bandwidth influence on the ToF random errors, case b.**

It should be noted that the pulse duration reduction will cause not only the bandwidth broadening, but also the energy decrease. Therefore, the ToF variance is decreasing with reduction of the bandwidth. In order to see only the bandwidth influence results should be corrected to maintain the energy amount constant. The results of constant energy investigation, when only the bandwidth is varied, are presented in Fig.9.
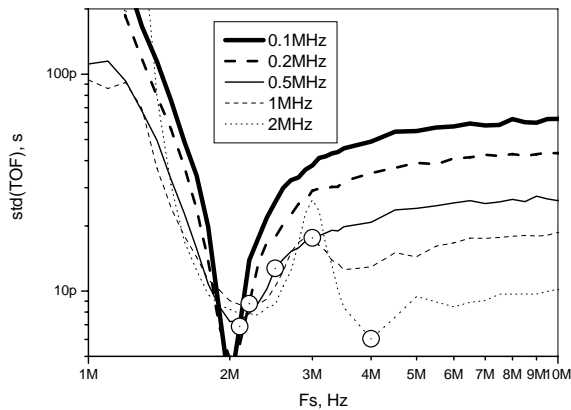

Fig. 9. **Bandwidth influence for a constant energy, case a.**

Now the results are in a good agreement with Eq. 10 predictions. The ToF standard deviation is increasing with bandwidth reduction for a constant energy but variable bandwidth simulations. The circles in Fig.9 indicate the double frequencies of the noise and signal power spectral density interception point (the same as indicated in Fig.3) for every individual case.

Eq. 17 implies that ADC quantization noise is related to ADC resolution and therefore the resolution should have a direct impact on the ToF variance. The numerical simulation has been carried out in order to evaluate the resolution impact on the ToF standard deviation for a large number (1000) of simulation runs. The obtained simulation results are presented in Fig.10.
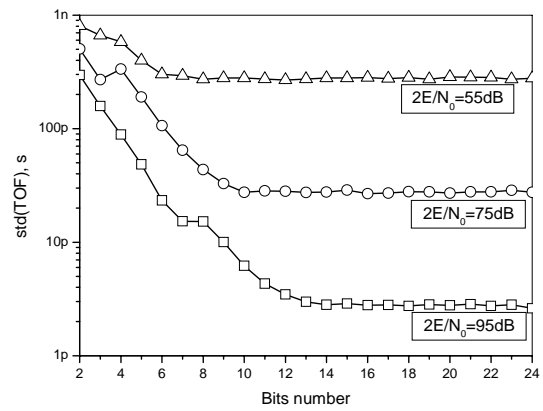

Fig. 10. **Bits influence on the ToF random errors, case a.**

Results for 55 dB, 75 dB and 95 dB SNR are presented. In order to get rid of sampling frequency induced errors, the sampling has been performed using a sufficiently high frequency f_{snorm} (100 MHz). For high SNR the resolution influence is significant. For comparison purposes it should be indicated that 95 dB correspond to 100 μV noise RMS value and 1V signal value: the indicated SNR are very high.

The curves in Fig. 10 contain a step at certain positions. In order to investigate the reason of this phenomenon sampling at 10 MHz has been performed. The comparison of 100 MHz and 10 MHz sampling frequencies are presented in Fig.11.
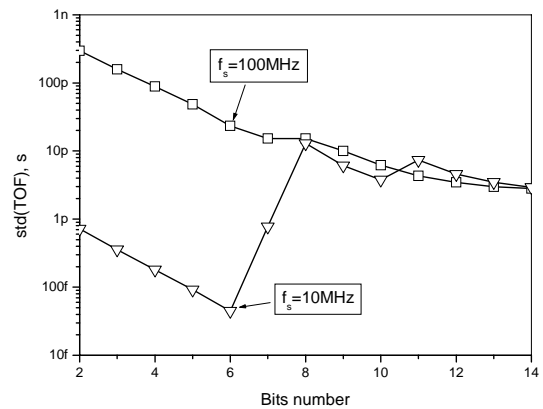

Fig. 11. **Bits influence together with a sampling rate, case a.**

It seems that for a low number of bits there is a significant random errors reduction. In order to verify the normalness of the distribution the lag-plot of the ToF values obtained at 6 bit and 10 MHz f_s ADC (for case a) has been investigated. The results are presented in Fig.12.
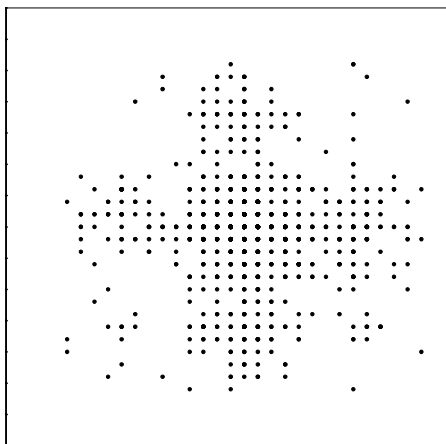

Fig. 12. **Lag-plot of the ToF values for f_s =10 MHz, case a.**

It turned out that the results contain a discrete structure (compare to the graph in Fig.5).

Conclusions

The accuracy of the time delay estimation using the direct correlation technique has been studied. Results of numerical simulation indicate that there is no necessity to choose a high sampling frequency for reduction of the ToF variance. The sampling rate as low as the double noise and signal power density interception point frequency is sufficient. Investigation of influence of ADC bits number revealed that there is a distortion of ToF distribution law at a low sampling frequency and resolution combinations.

The results are quite unexpected, therefore further experimental validation is necessary.

References

1. **Carter G. C.** (editor). Special issue on time delay estimation IEEE Trans. Acoust. Speech Signal Proc. Vol. 29. 1981.

2. **Tonga F., Tsoa S. K., Xub T. Z.** A high precision ultrasonic docking system used for automatic guided vehicle. Sensors and Actuators. 2005. Vol. 118. P.183–189.

3. TDC-GP1 General Purpose TDC. ACAM-messelectronic GmbH Blankenloch, Germany. 2001.

4. **Canali C., Cicco G., Morten B., Taronia A**. Temperature compensated ultrasonic sensor operating in air for distance and proximity measurements. IEEE Transactions on Industrial electronics. 1982. Vol. 29. No. 4. P. 336-341.

5. **Parrilla M., Anaya J. J., Fritsch C**. Digital signal processing techniques for high accuracy ultrasonic range Measurements. IEEE Trans. on Instrumentation and Measurement. 1991. Vol. 40(4). P. 759-763.

6. **Gueuning F., Varlan M., Eugene C., Dupuis P**. Accurate distance measurement by an autonomous ultrasonic system combining time-of-flight and phase-shift methods. IEEE Trans. on Instrumentation and Measurement. 1997. Vol.46. No.6. P.1236-1240.

7. **Nakahira K., Kodama T., Morita S., Okuma S**. Distance measurement by an ultrasonic system based on a digital polarity correlator. IEEE Trans. on Instrumentation and Measurement. 2001. Vol. 50. No. 6. P.1748-1752.

8. **Canhui C., Regtien P.** Accurate digital time-of-flight measurement using self-interference. IEEE Trans. on Instrumentation and Measurement. 1993. Vol. 42. No 6. P.990-994.

9. **Kestler W**. (editor). Analog-digital conversion. Analog devices; 2004.

10. **Dumbrava V., Svilainis L**. Ultrasonic data acquisition: sampling frequency versus bandwidth. Ultragarsas. 1998. Vol. 1(29). P. 29-33.

11. **Svilainis L., Dumbrava V**. Amplitude and phase measurement in acquisition systems. Matavimai. 2006. Vol. 2(38). P. 21-25.

12. **Jacovitti G., Scarano G.** Discrete time techniques for time delay estimation. IEEE Transactions on signal processing. 1993. Vol.41(2). P.525-533.

13. **Queir´os R.**, et.al. Cross-correlation and sine-fitting techniques for high resolution ultrasonic ranging. IMTC Instrumentation and Measurement Technology. Conference, Sorento. 2006. P. 552-556.

14. **Minkoff J.** Signal processing fundamentals and applications for communications and sensing systems. Norwood, MA, USA: Artech House. 2002.

15. **Quazi A. H**. An overview on the time delay estimate in active and passive systems for target localization. IEEE Trans. on acoustics, speech and signal processing .1981. Vol. 29(3). P 527-533.

16. **Girod B.**, et.al. Signals and systems. Chichester: John Wiley& Sons. 2001.

17. **Svilainis L., Dumbrava V.** Design of a low noise preamplifier for ultrasonic transducer. Ultragarsas. 2005. Vol. 2(55). P.28-32.

18. **Lai X. and Torp H.** Interpolation methods for time-delay estimation using cross-correlation method for blood velocity measurement. IEEE transactions on ultrasonics, ferroelectrics, and frequency control. 1999. Vol.46. No.2. P.277-290.

19. **Kazys R.** Delay time estimation using the Hilbert transform. Matavimai. 1996. Vol.3. P.42-46.

L. Svilainis, V. Dumbrava

Diskretizavimo parametrų įtaka sklidimo laiko įvertinimo tikslumui

Reziumė

Nagrinėjami skaitmeninių ultragarsinių sistemų atspindėto signalo vėlinimo laiko įvertinimo klausimai. Aptariami vėlinimo laiko matavimo ir įvertinimo metodai. Pateikiamos diskrečiosios matematinės išraiškos šiam laikui teoriškai įvertinti. Aptariami skaitmeniniai eksperimentai, atlikti keičiant sistemoje veikiančio baltojo triukšmo spektrinį tankį, diskretizavimo dažnį, skaitmeninio analogo keitiklio skilčių skaičių, zonduojančio signalo centrinį dažnį ir juostos plotį.